

Article

Epoxy Coatings Doped with (3-Aminopropyl)triethoxysilane-Modified Silica Nanoparticles for Anti-Corrosion Protection of Zinc

Tamara-Rita Ovari ¹, Timea Toth ², Gabriel Katona ² , Gabriella Stefánia Szabó ^{2,*}  and Liana Maria Muresan ¹

¹ Department of Chemical Engineering, Faculty of Chemistry and Chemical Engineering, Babes-Bolyai University, 11 Arany J. Street, 400028 Cluj-Napoca, Romania; tamara.ovari@ubbcluj.ro (T.-R.O.)

² Department of Chemistry and Chemical Engineering of the Hungarian Line, Faculty of Chemistry and Chemical Engineering, Babes-Bolyai University, 11 Arany J. Street, 400028 Cluj-Napoca, Romania

* Correspondence: gabriella.szabo@ubbcluj.ro

Abstract: Epoxy (EP) coatings containing silica (SiO₂) and (3-Aminopropyl)triethoxysilane-modified silica (SiO₂-APTES) nanoparticles were prepared via the dip-coating technique on a zinc substrate. A detailed study was performed regarding their incorporation into the matrix, followed by the investigation of the newly obtained organic–inorganic hybrid coatings’ anti-corrosive properties. The two methods of embedding the nanoparticles were (I) modification of the silica nanoparticles with APTES followed by their introduction into the epoxy resin, and (II) functionalization of the silica nanoparticles in the epoxy gel before the addition of the hardener. It was observed that through the second method, the coating was homogeneous, with no sign of agglomerates. The nanoparticles were subjected to morpho-structural and physical–chemical analysis using Fourier-Transform Infrared Spectroscopy and Transmission Electron Microscopy, while the coatings were examined through Scanning Electron Microscopy and Energy-Dispersive X-Ray Spectroscopy, contact angle measurements and adhesion tests. The anti-corrosive performance of epoxy-coated zinc was analyzed using electrochemical impedance spectroscopy and polarization curves to investigate the impact of silanized SiO₂ nanoparticle incorporation. Based on long-term corrosion testing, the epoxy-SiO₂-APTES composite coatings showed a higher corrosion resistance than the undoped epoxy layer.

Keywords: epoxy coating; silica nanoparticles incorporation; corrosion; electrochemical impedance spectroscopy



Citation: Ovari, T.-R.; Toth, T.; Katona, G.; Szabó, G.S.; Muresan, L.M. Epoxy Coatings Doped with (3-Aminopropyl)triethoxysilane-Modified Silica Nanoparticles for Anti-Corrosion Protection of Zinc. *Coatings* **2023**, *13*, 1844. <https://doi.org/10.3390/coatings13111844>

Academic Editor: Florina Branzoi

Received: 25 September 2023

Revised: 21 October 2023

Accepted: 23 October 2023

Published: 27 October 2023



Copyright: © 2023 by the authors. Licensee MDPI, Basel, Switzerland. This article is an open access article distributed under the terms and conditions of the Creative Commons Attribution (CC BY) license (<https://creativecommons.org/licenses/by/4.0/>).

1. Introduction

Despite great efforts and innovations, the corrosion of metals continues to pose a great challenge to countries’ economies. In order to eliminate this drawback, many efficient solutions were created, most of which were based on the protection of metal surfaces with some kind of coating. Unfortunately, some of them did not prove to be successful in terms of environmental and health aspects (e.g., chromate conversion coatings). Therefore, continuous development is still necessary. Countless environmentally friendly coatings have come to the fore in recent times. Among these, we can mention the organic, biopolymer-based, inorganic and metallic ones [1–4]. Although the goal may be to synthesize new, more performant layer formers that provide better protection to metals, the development of already known and tested materials by eliminating their disadvantageous properties may be just as effective.

Epoxy (EP) is one of the most popular coating matrix materials due to its good adhesion, high corrosion and heat resistance [5]. At the same time, due to its high moisture absorption and rigidity, which lead to the formation of cracks, its barrier effect deteriorates in the long term. Coatings’ performance can be enhanced and even self-healing properties

achieved through the incorporation of organic, inorganic or hybrid nanoparticles into the polymer matrix. The most used can be listed, without claiming to be complete: graphene [6], graphene oxide [7,8], silica and their functionalized derivatives [9–11].

Permeability can be reduced by increasing the cross-linking of the polymer resin through covalent bond formation between the epoxy groups and the functional groups of the nanosized fillers. The incorporation of graphene oxide (GO) [12] and its derivatives, obtained through its functionalization using amino-group-containing compounds [13–16], can provide composites with diminished permeability and enhanced barrier properties. In addition, increased adhesion to the substrate is achieved through bonds formed with metal oxides on the surface. GO can also be used as nanocontainer for Ce-metal–organic–framework nanoparticles [17], and after that added to epoxy. Suitable materials for improving mechanical properties, such as increasing fracture toughness, are functionalized GO with silica [18] or with bisphenol-A [19].

Inorganic nanosized-particle-incorporated organic polymers are generally named hybrid composites [20]. Their enhanced properties are due to the high chemical and thermal stability of the inorganic component and the processability of the organic polymer. Silica (SiO_2) is one such environmentally friendly, widely used inorganic compound, with increased anti-corrosion effects. Silica coatings can be obtained in a gentle, harmless sol–gel transformation from alkoxy silane precursor sols [21,22] on different shaped substrates. At the same time, mesoporous structures can be obtained by using different surfactants as template formers, in which corrosion inhibitors can be stored [23]. Also, the silica network can be doped [24] or reinforced using organic inhibitors, providing less porous and increased corrosion-resisting coatings [25].

Silica nanoparticles (NPs) can be obtained using the Stöber sol–gel method [20]. A silica-NP-doped epoxy matrix was found to be more hydrophobic, with improved microstructure and increased hardness [11]. A main issue that remains in the preparation of hybrid composites is good dispersion of the NPs in the polymer matrix, which can be achieved via surface functionalization of the NPs [10,26]. In their works, the authors highlighted the uniform distribution of NPs in the coating and good adhesion of the layers to the metallic substrate (usually provided by amino groups) as necessary conditions to enhance their anti-corrosion behavior.

Another goal of designing anti-corrosion coatings is the development of self-healing properties, which can also be achieved by functionalizing the NPs [9,26,27]. Amino-functionalized hybrid silica–epoxy coatings, besides having a better adherence to the surface, diminished the NP agglomeration and reduced the moisture pathway in the coating, consequently increasing the anti-corrosion resistance.

There are reported green synthesis methods for obtaining waterborne epoxy smart coatings [28–30]. Although there is a great effort to introduce environmentally friendly technologies, the task to be solved for the time being is to ensure the durability of the epoxy polymers obtained in this way [31].

In the present work, two different methods for the preparation of (3-Aminopropyl)triethoxysilane-modified silica (SiO_2 -APTES) NPs are proposed. After NP incorporation in the EP matrix, the obtained coatings prepared on zinc (Zn) substrates via dip coating were thoroughly characterized. The aim of the comparative study was to establish the conditions for the production of the best anti-corrosion coating suitable for saline environments, as encountered in marine transportation or during the winter season when brine solutions are frequently employed.

2. Materials and Methods

2.1. Materials

The materials used in this work were Primer FM epoxy resin (component A) and hardener (component B) from MAPEI Romania (Bucharest, Romania); silicon dioxide (SiO_2) nanopowder and tetraethyl orthosilicate (TEOS) from Sigma-Aldrich (St. Louis, MO, USA); (3-Aminopropyl)triethoxysilane (APTES) from Alfa Aesar (Haverhill, MA,

USA); tetrahydrofuran (THF) from POCH, Gliwice, Poland; acetone, isopropanol and ethanol (EtOH) from CHEMICAL Company (Iasi, Romania); potassium chloride (KCl) from Primexchim (Bucharest, Romania); and hydrogen chloride (HCl) (35–38% concentration) and sodium chloride (NaCl) were purchased from Chempur (Karlsruhe, Germany). The zinc plates, with a purity of 99%, containing reduced amounts of Ti and Cu, were purchased from Altdepozit (Galati, Romania).

2.2. Methods

In order to highlight bond formation between modified SiO₂ NPs and APTES, Fourier-Transform Infrared Spectroscopy (FT-IR) spectra were recorded. A JASCO FT/IR-6800 spectrometer was employed within the spectrum of 500–4000 cm⁻¹. The FT-IR measurements were performed in solid state.

Transmission Electron Microscopy (TEM) measurements were conducted with a Hitachi H-7650 transmission electron microscope. The dispersion process of the nanoparticles took place in ethanol.

The coatings' adhesion was affirmed through the cross-hatch adhesion test employing an Elcometer Cross Hatch Adhesion Tester and categorized following the ASTM D3359 Classification [32]. A 7 × 7 surface area was employed, and the percentage of the area remaining after tape removal was assessed.

Contact angle measurements of the coated zinc substrates were realized to obtain data regarding the polarity of the coatings. The measurements were conducted in a closed sample chamber, in saturated atmosphere, with 20 µL distilled water droplets. The contact angle was determined using the ImageJ software, with an uncertainty of ±0.1.

A Hitachi SU8230 ultra-high-resolution Scanning Electron Microscope (SEM) was used to study the morphological and structural properties of the coated samples, with Energy-Dispersive X-ray Spectroscopy (EDS) graphs.

The electrochemical measurements (OCP—open-circuit-potential measurements; EIS—electrochemical impedance spectroscopy; and PDP—polarization measurements) were carried out in a 3-electrode cell, composed of a working electrode (WE—bare zinc plates possessing an active area of 2 cm²), a counter electrode (CE—platinum wire) and a reference electrode (RE—Ag/AgCl/KCl_{sat}). The zinc plates were masked with lacquer to expose a 2 × 1 cm² surface. All experiments were conducted in 3 wt% NaCl aqueous solution. OCP measurements were carried out for 30 min each, representing the stabilization time of the samples in the electrolyte, to obtain a corrosion potential (E_{corr}) as a reference value for further analyses. EIS measurements were conducted within a 10 mHz–10 kHz frequency interval, with a sinusoidal current of 10 mV amplitude. The equivalent electrical circuit was fitted and the results were processed with ZSimpWin software. Potentiodynamic polarization (PDP) measurements were performed at E = ±200 mV vs. OCP, at a scan rate of 1 mV/min. Three repetitions of each experiment were conducted to assess reproducibility. Equation (1) was used to calculate the inhibition efficiency (IE) of the coated Zn samples:

$$IE(\%) = \frac{i_{\text{corr}}^0 - i_{\text{corr}}}{i_{\text{corr}}^0} \times 100 \quad (1)$$

where i_{corr}^0 represents the corrosion current of the blank sample and i_{corr} the corrosion current of the nanoparticle-filled samples.

The wet/dry testing involved immersing the samples in the corrosive medium for 1 h, followed by 24 h of drying, after which the impedance was measured.

2.3. Functionalization of the SiO₂ Nanoparticles

The functionalization of the SiO₂ NPs was carried out 2 different ways (Figure 1).

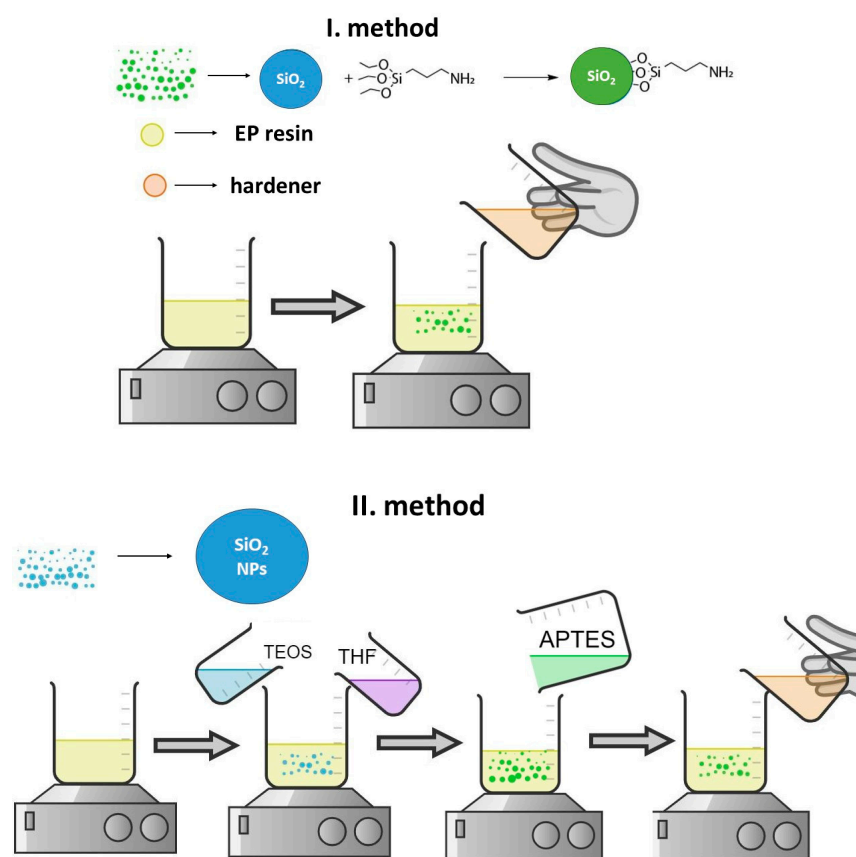


Figure 1. Graphical illustration of the two preparation methods of SiO₂-APTES NPs.

Method (I): 0.5 g of SiO₂ nanopowder was added to a 95:5 (weight) ethanol/water mixture, then placed in an ultrasonic bath for 10 min to achieve a better dispersion. An amount of 1 g of APTES was added into the system and the mixture was subjected to an additional 5 min of ultrasonication, followed by stirring for 2 h at 70 °C, and then filtered, washed with distilled water and dried at room temperature before application [33].

Method (II): SiO₂ nanoparticle modification with APTES was used for EP resin component A. To 21.5 g of EP, 0.28 g of SiO₂ nanoparticles, 0.155 mL of tetraethyl orthosilicate (TEOS) and 15 mL of tetrahydrofuran (THF) were added, followed by stirring for 2 h at 60 °C. Then, 0.01 mL of APTES was added, followed by another 2 h of stirring at 60 °C. An amount of 0.04 mL of sulfuric acid–water mixture with a pH of 2 was introduced under ongoing stirring, continuing the stirring process for additional 4 h [26].

2.4. Coatings' Preparation

The first step in preparing the samples was to prepare and clean the zinc plates. The plates were carefully sanded with emery paper (P1000, P2000, P5000), which was followed by a surface treatment applied with isopropanol wipes, then 0.1 M HCl solution, and then the plates were rinsed with distilled water and then degreased with isopropanol.

The epoxy (bisphenol A epoxy resin) precursor was made of two components: component A—the epoxy itself—and component B—the hardener (a mixture of amine-containing monomers and oligomers). Beside the EP samples, the resin contained 1% of SiO₂ nanoparticles [34], which were mixed into the hardener ensuring a uniform distribution using an ultrasonic bath. The next step involved mixing the two components in a 3:1 ratio via mechanical stirring. It took 90 min for the EP to enter the gel-like form, where the curing was only partial, but already lost its workability. To accomplish the ultimate curing process, the samples were left for 4 days at room temperature to fully cure. It is important to note that in the case of the second functionalization method, the prepared samples were first

heat-treated at 100 °C for 4 h, followed by a 4-day curing period at room temperature. Carrying out the initial curing at this temperature is necessary to evaporate the THF solvent from the coatings obtained via the SiO₂-APTES (II. method).

3. Results and Discussion

3.1. Characterization of the Silica Nanoparticles

In order to put in evidence the functionalization of SiO₂ NPs, Fourier-Transform Infrared Spectroscopy (FT-IR) spectra were recorded. From these spectra (Figure 2), it can be observed that in the range of 470–1100 cm⁻¹, the Si-O-Si vibrations exhibit a strong signal, which was due to the silica phase. In the spectrum of SiO₂, the signal of the silanol -OH was visible in the range of 3200–3500 cm⁻¹. Comparing the FT-IR spectra of SiO₂ and the APTES-modified SiO₂ (I), in the SiO₂-APTES (I) spectra we can see that peaks at around 3000 cm⁻¹ attributed to the APTES C-H bonds, and at 3450 cm⁻¹ the terminal N-H groups were overlapped with the -OH of the silanol.

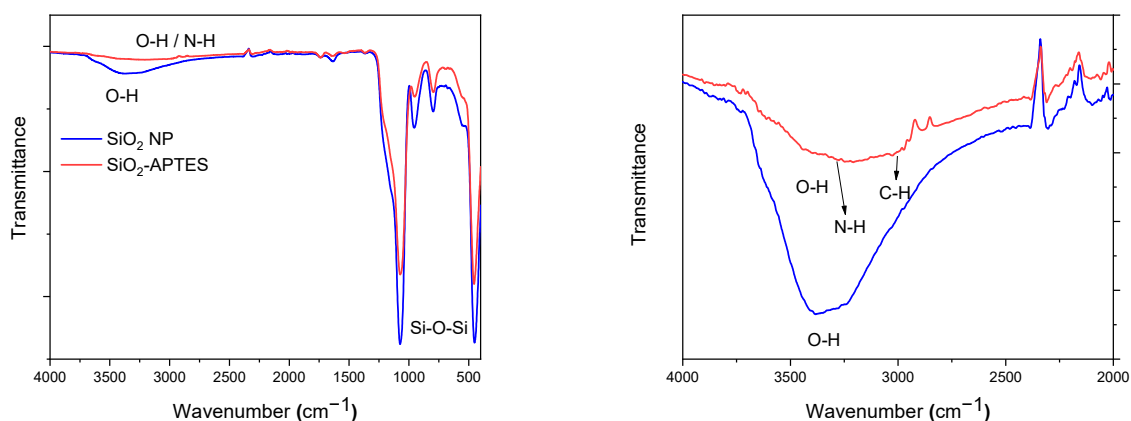


Figure 2. The FT-IR spectra of commercially purchased SiO₂ NP and SiO₂ modified with APTES (I).

We can deduce that the reaction indeed took place; the APTES molecules were attached to the terminal oxygens of SiO₂, forming terminal -NH₂ groups. This interpretation aligns with similar evaluations presented in the literature [35].

The Transmission Electron Microscopy (TEM) images of the nanoparticles are presented in Figure 3. The clearly drawn conclusion from these images was that through the APTES functionalization of the SiO₂, the particle size and the possibility of agglomeration can be reduced. In case of SiO₂ the particle size ranges between ~42 and 53 nm (Figure 3A), while the SiO₂-APTES (I) nanoparticles' length varies from 14 nm to 22 nm (Figure 3B). This phenomenon can be attributed to the presence of APTES molecules within the silica's structure, effectively preventing nanoparticle aggregation. Surface modification thus facilitates a more uniform distribution of the particles in the epoxy resin, significantly enhancing the properties of the corrosion-resistant coatings.

3.2. Coatings Characterization

3.2.1. Thickness Measurements

The thickness measurements of the epoxy-based layer coatings (Figure 4) showed that there was no significant difference between the EP coating and the EP layers containing SiO₂ NPs or APTES-functionalized NPs using method (I). All of them measured ~25 μm. On the contrary, a significant difference can be observed in the case where the SiO₂ was modified with APTES directly in the epoxy resin (method II), where tetrahydrofuran (THF) solvent was used for dilution of epoxy resin. In this scenario, the coatings' thickness reached only 12 μm.

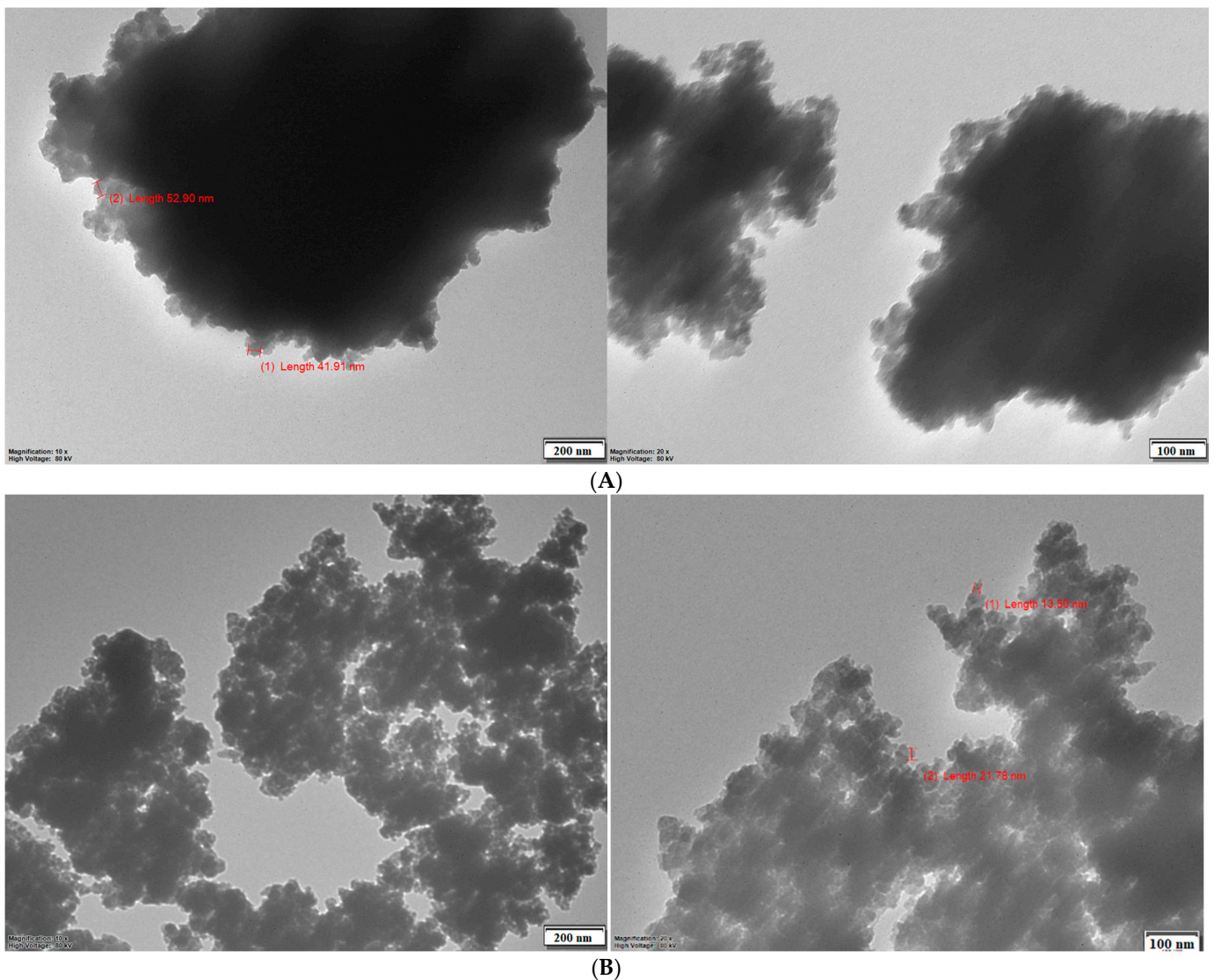


Figure 3. TEM images of commercially purchased SiO₂ NPs (A) and APTES-modified SiO₂ NPs (I. method) (B).

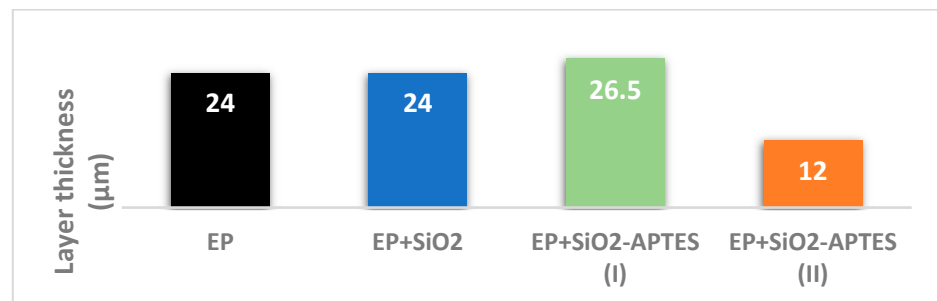


Figure 4. The studied EP coatings’ thickness with and without SiO₂ NP.

3.2.2. Adhesion Tests

After measuring the layers’ thickness, the samples underwent adhesion tests. The adhesion of different layers is illustrated in Figure 5. While the epoxy resin without any filler shows weak results, maintaining only 61% of the studied square after the test, it can be observed that all three fillers significantly improved the layers’ adhesion. This confirms

the literature data mentioning that the presence of amine groups increases adhesion to the metal substrate [9].

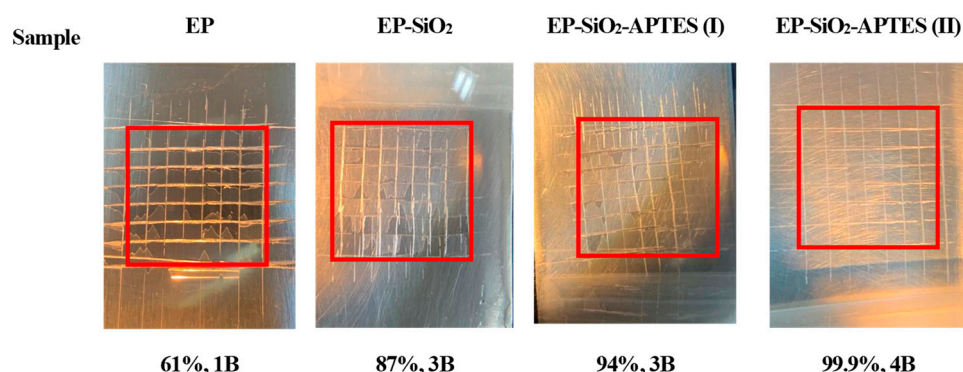


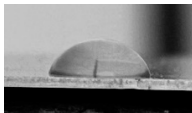
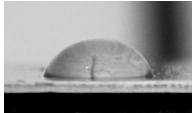
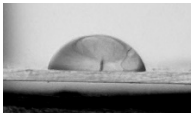
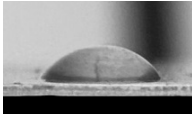
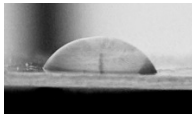
Figure 5. Cross-hatch adhesion test results for coated samples. The 7×7 red rectangles show the surface from which adhesion was calculated (percentages). Followed by the ASTM D3359 Classification.

Particularly notable was the EP-SiO₂-APTES (II), which exhibited almost 100% adhesion, even if its thickness was smaller than that of the other coatings.

3.2.3. Contact Angle Measurements

The hydrophilic nature of epoxy resin is an unfavorable factor influencing its anti-corrosion properties because the hydrophilic resin layer absorbs the electrolyte solution, which, if it reaches the zinc substrate, significantly damages it. Therefore, by incorporating nanofillers into the matrix, it can be anticipated that they will influence the contact angle measurements of the samples by lengthening the pathway of the electrolyte, thereby decreasing the hydrophilic nature of the coatings. It can be observed (Table 1) that due to SiO₂-APTES incorporation into the EP matrix, the contact angle values are higher and this indicates a less hydrophilic surface. The fact, in the case of SiO₂-APTES (II), that after a period of time the smallest reduction in contact angle can be observed suggests that the coating in this case has a lower permeability and less hydrophilicity. Moreover, in Section 3.2.4 of the SEM/EDS images, it is evident that the SiO₂-APTES II method yields the highest coating uniformity with no agglomerates. The obtained values are in good agreement with those reported in the literature so far regarding EP coatings [36].

Table 1. Results of contact angle measurements for EP, EP/SiO₂, EP/SiO₂-APTES (I) and (II) layers, at 0 and 30 min intervals, with a 20 μ L droplet of distilled water.

Sample	EP	EP-SiO ₂	EP-SiO ₂ -APTES (I)	EP-SiO ₂ -APTES (II)
				
0 min	70°	70°	74°	83°
				
After 30 min	56°	58°	64°	74°

The outcomes of adhesion and contact angle results emphasize the importance of how nanofillers were integrated. The unmodified SiO₂ could form agglomerates in the EP

coating, in such places possibly enhancing the channeling of the electrolyte towards the substrate and increasing the occurrence of corrosion. Under these conditions, the beneficial effect of NPs cannot be maximized. The APTES functionalization adjusted the adhesion results and decreased the hydrophilic nature of the layers.

3.2.4. Scanning Electron Microscopy (SEM)

As the uniformity of the different coatings is a key element in their protective ability, the coated Zn samples were investigated via SEM and EDS. The SEM images of the samples (Figure 6) proved that by modifying the SiO₂ nanoparticles within the epoxy resin, we achieved a more uniform coating, eliminating the chance of aggregations. The repartition of the SiO₂ NPs inside the epoxy matrix was more uniform in the particular case when they were modified with APTES using method II (Figure 7).

3.3. Electrochemical Investigation of the Coatings

In order to put in evidence the anti-corrosion resistance of the various coatings, the samples were investigated via electrochemical methods. One well-established method of evaluating electrochemical impedance spectroscopy (EIS) spectra is by fitting equivalent circuits [37]. The absolute impedance ($|Z|_{0.01\text{Hz}}$) and the breakpoint frequency values (F_b) were determined from Bode plots and other electrochemical parameters were extracted by fitting the proper equivalent electrical circuit (EC) to the sample's behavior (Figure 8). For the uncoated Zn sample, a $R_s(Q_{dl}R_{ct})$ circuit fitted the best with a single constant phase element (CPE) representing a non-ideal charge transfer at the substrate–electrolyte interface, where R_s stands for the resistance of the electrolyte, Q_{dl} for the double-layer capacitance and R_{ct} for the charge transfer resistance (Figure 8C). In case of the EP-coated Zn electrode, another CPE connected in series and composed of a Q_{coat} capacitance and R_{coat} resistance was present due to the deposited organic layer (Figure 8D). When the EP matrix was embedded with SiO₂ NPs, the connection of the ($Q_{coat}R_{coat}$) pair best fitted in parallel (Figure 8E).

The values of $|Z|_{0.01\text{ Hz}}$ depicted in Table 2 indicate modest results in the case of bare Zn and much better ones in the case of coated samples. The impedance modulus exceeding $10^6 \Omega$ at the low frequency of 0.01 Hz indicates a good barrier performance of the coating [38]. The highest values were noticed for Zn/EP-SiO₂-APTES (II) samples, confirming once again their better quality and the highest corrosion resistance.

Table 2. $|Z|_{0.01\text{Hz}}$ values for the different coated Zn samples extracted from Bode diagrams.

Sample	Zn	EP	EP-SiO ₂	EP-SiO ₂ -APTES (I)	EP-SiO ₂ -APTES (II)
$ Z _{0.01\text{Hz}}$ (kΩ)	1.67	2.14×10^3	3.72×10^3	5.58×10^3	8.95×10^3

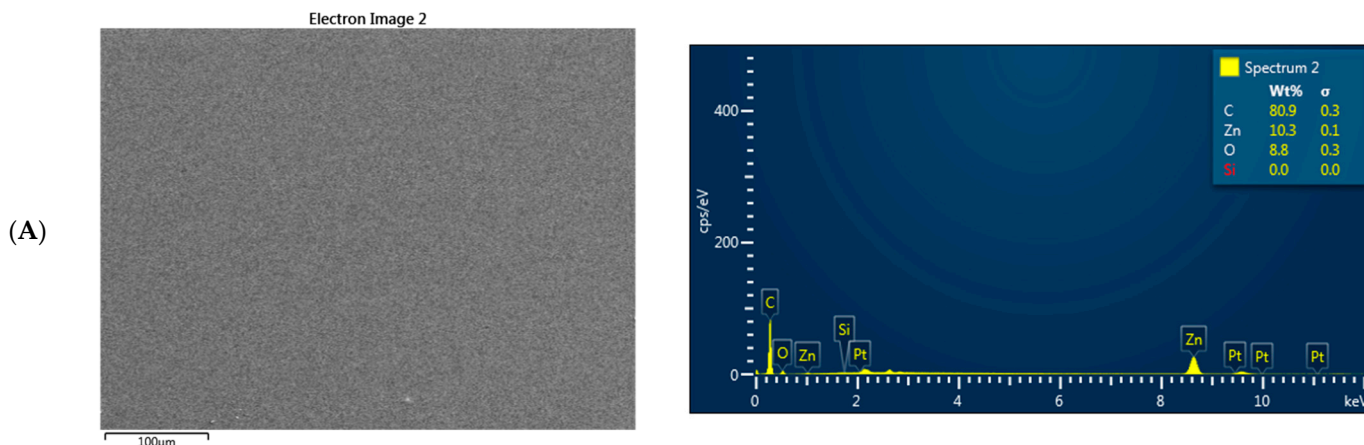


Figure 6. Cont.

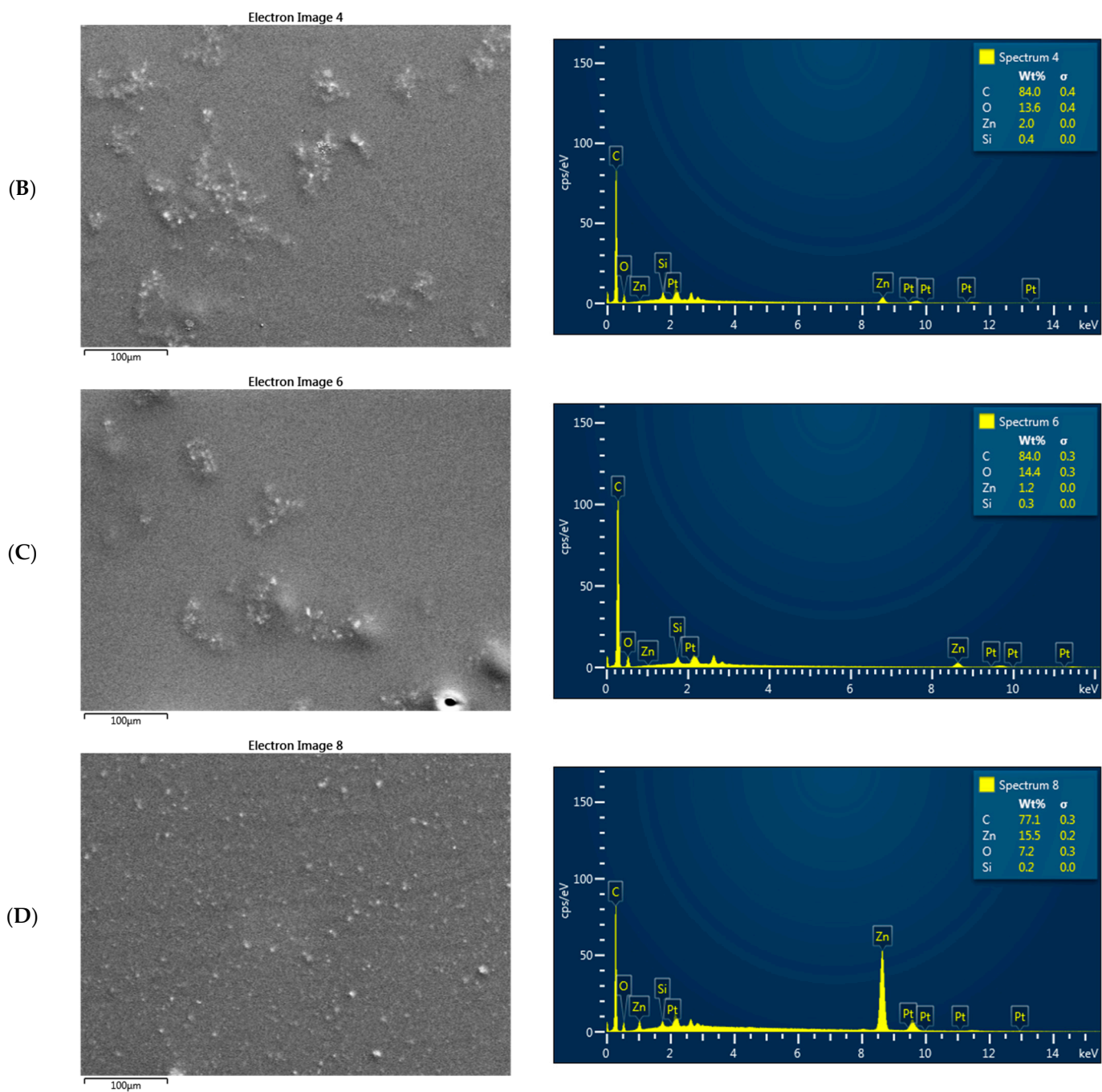


Figure 6. SEM images (left) and EDS graphs (right) of EP (A), EP-SiO₂ (B), EP-SiO₂-APTES (I) (C) and EP-SiO₂-APTES (II) (D).

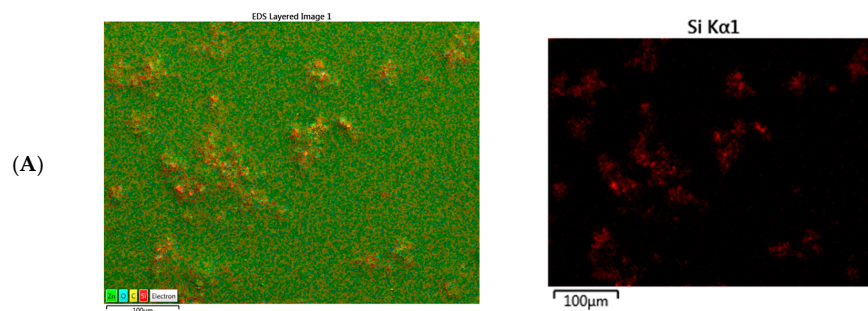


Figure 7. Cont.

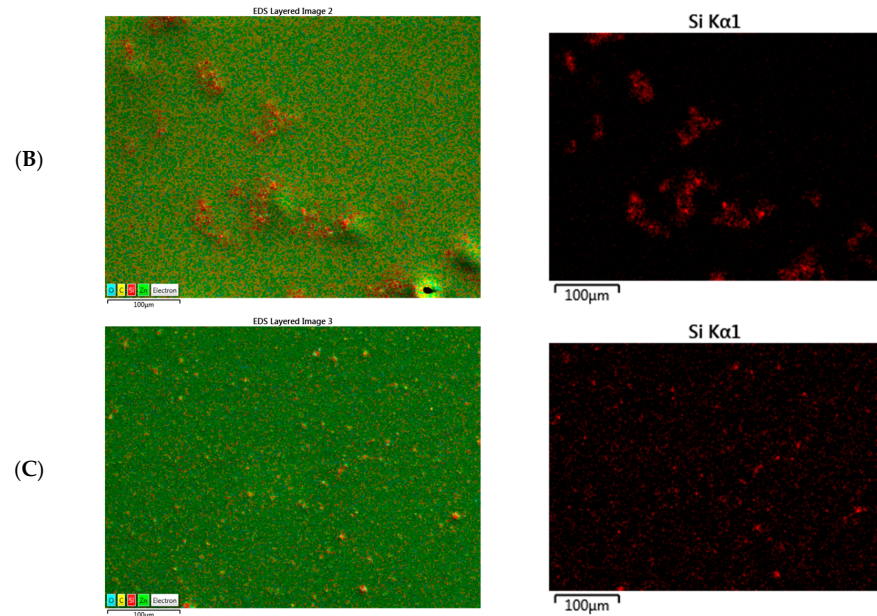


Figure 7. SEM/EDS silicon mapping of EP-SiO₂ (A), EP-SiO₂-APTES (I) (B) and EP-SiO₂-APTES (II) (C).

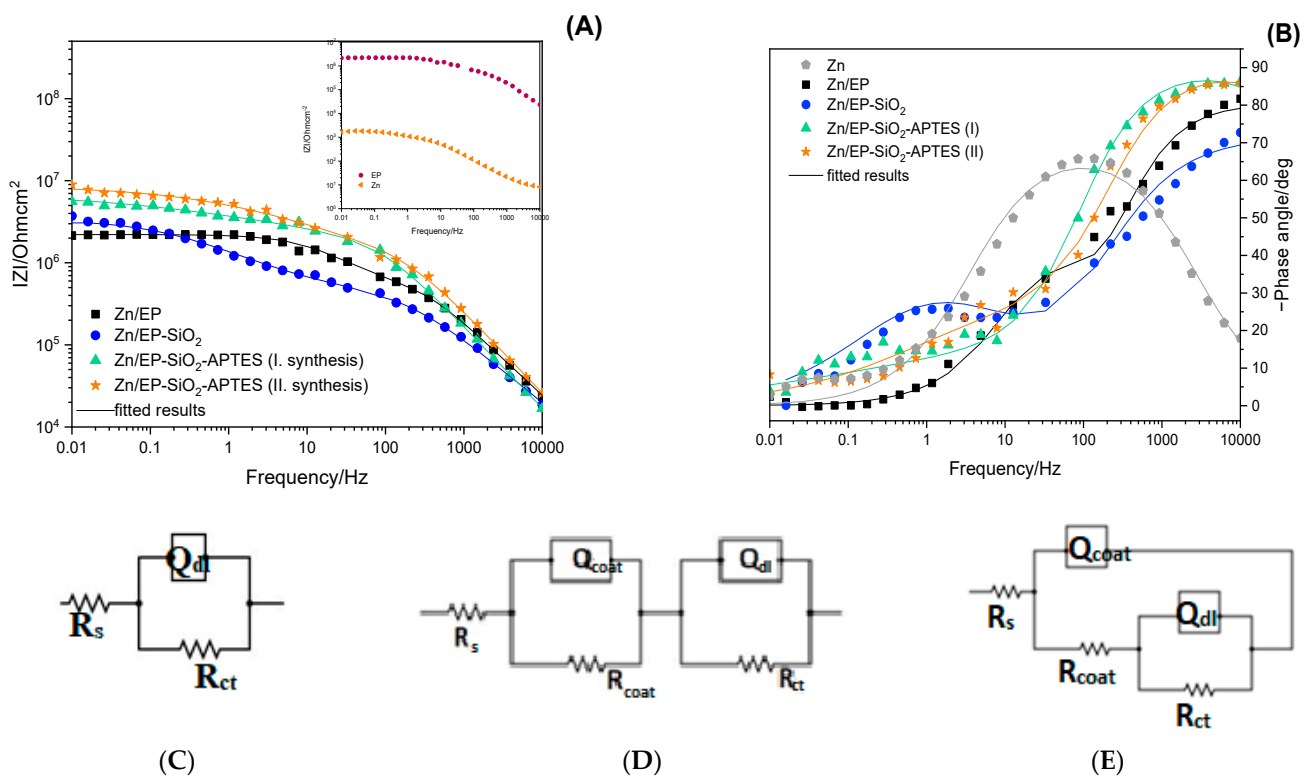


Figure 8. Bode diagrams illustrating the absolute impedance (A) and the phase angle (B) of uncoated Zn sample, Zn/EP, Zn/EP SiO₂ used as a filler, Zn/EP-SiO₂-APTES (I) and Zn/EP-SiO₂-APTES (II) samples, and the corresponding fitted electrical equivalent circuits (C–E), respectively.

The electrochemical parameters extracted from the impedance diagrams using the EC presented in Figure 7 (Table 3) show that the R_p significantly increased in the case of EP coating containing APTES-modified SiO₂ NPs. The most resistant was proven to be Zn/EP-SiO₂-APTES (II). The coating's Q_{coat} decreased by one order of magnitude in the presence of SiO₂ nanofillers, and by two orders of magnitude in the case of APTES-modified

SiO₂ nanoparticles (I) and (II). As the coating absorbs water, its effective dielectric constant rises, leading to an increase in the capacitance of the coating. The initial phase of coating degradation is characterized by the absorption of water [39].

Table 3. Electrochemical parameters values of the uncoated Zn and EP-coated Zn with and without nanofillers.

Sample	R _s (kΩ cm ²)	10 ³ × Q _{coat} (μSs ⁿ)	n	R _{coat} (kΩ cm ²)	10 ¹ × Q _{dl} (μSs ⁿ)	n	R _{ct} (kΩ cm ²)	R _p = R _{coat} + R _{ct} (kΩ cm ²)	10 ³ × Chi ²
Zn	0.01	-	-	-	731.0	0.8	1.20	1.20	7.63
Zn/EP	0.39	15.80	0.8	1789	0.019	0.9	428	2217	3.09
Zn/EP-SiO ₂	1.40	7.630	0.8	497	2.590	0.6	2918	3415	7.15
Zn/EP-SiO ₂ -APTES (I)	1.32	0.940	0.9	1176	1.300	0.7	6042	7218	6.87
Zn/EP-SiO ₂ -APTES (II)	1.41	0.613	1	1171	0.524	0.7	7014	8185	9.10

The weakening of the resistance to corrosion can also be monitored using graphical analysis techniques [38,40] and studying the breakpoint frequencies [41–44]. The stability of the developed coatings was investigated via the breakpoint frequency (F_b), defined as the frequency at the −45° phase angle. The area under the Bode plots delimited by F_b and impedance modulus |Z| allows us to recognize if a failure occurs in the coating. When the area under the plot is fully capacitive, the coating is considered intact. Corrosion starts when the area is a combination of capacitive and resistive regions, and failure occurs when the whole area is of a resistive nature [45]. When determining the F_b in our case, two regions appear on the diagrams (Figure 9): A₁, marked in gray, which represents the resistive region, and A₂, marked in green, representing the capacitive region. The size of the capacitive region, marked as A₂, indicates the protective capacity of the layer. The larger the area, the better the protection provided by the respective layer. On the other hand, a shift in F_b toward higher frequencies is associated with a vulnerability of the coating. Thus, when producing coatings, the goal is to increase the size of the capacitive region, and in the meantime reduce the size of the resistive region.

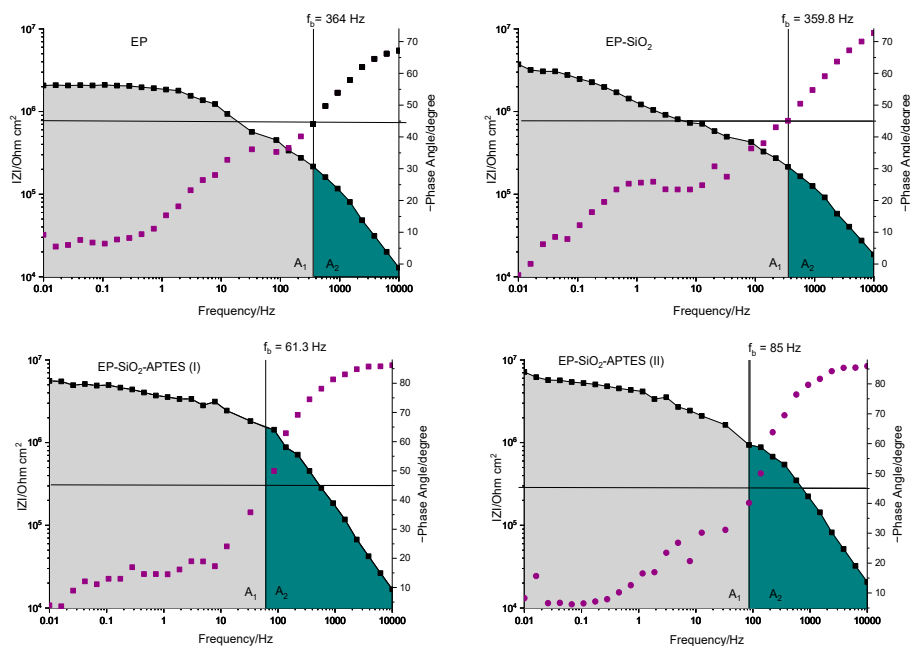


Figure 9. The breakpoint frequency of EP resin layers filled with SiO₂ NPs.

Figure 9 illustrates the growth of the capacitive region in the case of epoxy resin layers filled with APTES-modified SiO₂ NPs, improving the layers' protective capability. A noticeable change in the F_b value can be observed. While in the case of unmodified SiO₂ nanoparticles, this value was 359.8 Hz on a logarithmic scale, the F_b of the EP layer doped with SiO₂ modified with APTES was approximately 61 Hz, and, respectively, 85 Hz. An increase in the A₂ area when SiO₂ and modified SiO₂ NPs were embedded in EP clearly suggests an improvement in the corrosion resistance of the coatings.

After verifying the long-term corrosion resistance of the samples, one can conclude that in the case of all EP-based samples, their resistance deteriorates quickly after exposure to NaCl electrolytes due to their hydrophilic nature (Figure 10 and Table 4). After 2 days, the EP nearly loses its protective ability. However, the EP layers doped with SiO₂ nanoparticles, especially those modified with APTES, degrade at a slower rate. This can be attributed to the nanoparticles filling the pores of the EP, thereby extending the diffusion path of the corrosive medium. After 2 days of immersion, the |Z|_{0.01Hz} value for the EP-SiO₂-APTES layer was two orders of magnitude higher than that of the plain EP layer. The APTES-modified SiO₂ NPs system (where the synthesis took place directly in the EP resin, method II) still showed a value of $2.18 \times 10^5 \Omega$ after 2 days of continuous immersion. Possible explanations for this include the better homogeneity of the coating and the agglomeration-free distribution of particles, as shown in SEM/EDS micrographs (Figures 6 and 7), despite the significantly smaller layer thickness in this case.

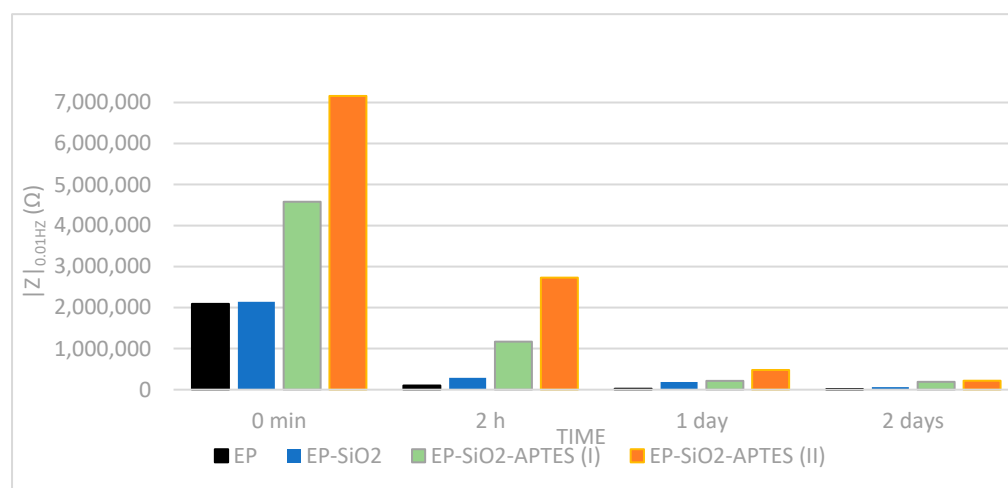


Figure 10. Graphical representation of |Z|_{0.01Hz} values for the investigated samples during 2 days of measurements in 3 wt% NaCl corrosive solution.

Table 4. |Z|_{0.01Hz} values for the investigated samples during 2 days of measurements in 3 wt% NaCl corrosive solution.

Sample	0 min	2 h	1 Day	2 Day
EP				
Z _{0.01Hz} (Ω)	2.09×10^6	1.01×10^5	1.99×10^4	8.40×10^3
EP-SiO ₂				
Z _{0.01Hz} (Ω)	2.14×10^6	2.86×10^5	1.85×10^5	6.01×10^4
EP-SiO ₂ -APTES (I)				
Z _{0.01Hz} (Ω)	4.58×10^6	1.05×10^6	2.11×10^5	1.90×10^5
EP-SiO ₂ -APTES (II)				
Z _{0.01Hz} (Ω)	7.16×10^6	2.73×10^6	4.80×10^5	2.18×10^5

This continuous exposure to the highly corrosive NaCl environment is more representative of the corrosion protection in sea water than in a real marine atmosphere. Therefore, wet/dry testing was also conducted for 7 days. As depicted in Figure 11, the EP and SiO₂-doped layers exhibited a more pronounced decline in absolute impedance, falling below 10⁶ Ω after 3 days, with a steeper slope. In contrast, the APTES-modified SiO₂-doped coatings displayed a more gradual reduction, particularly with method II, retaining a $|Z|_{0.01\text{Hz}}$ value of 5200 kΩ after 7 days.

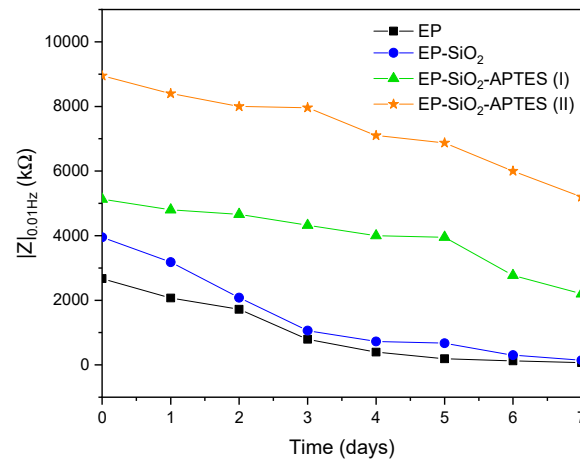


Figure 11. Graphical illustration of $|Z|_{0.01\text{Hz}}$ values for the samples subjected to wet/dry testing over a 7-day duration.

The results obtained from the impedance measurements were in agreement with those extracted from the polarization curve measurements (Figure 12 and Table 5). The lowest i_{corr} values and the highest inhibition efficiency were noticed in the case of the Zn/EP-SiO₂-APTES (II) coating. The uniform distribution, increased adhesion and decreased hydrophilicity of the APTES-functionalized SiO₂ NPs collectively led to a low i_{corr} of 0.75 μA/cm².

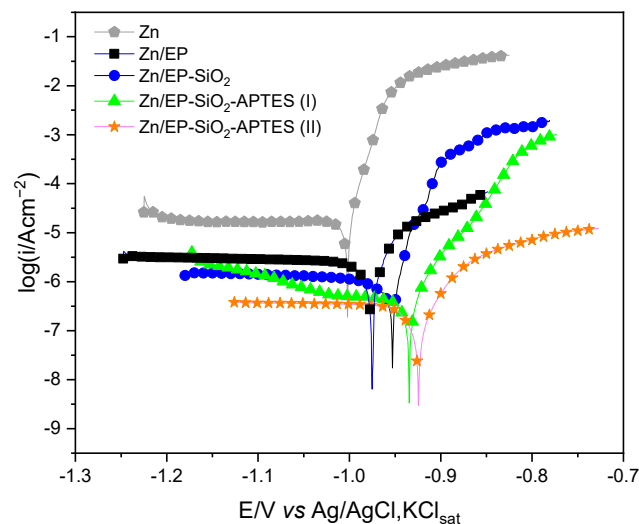


Figure 12. Polarization curves for bare Zn and for coated Zn substrates recorded in 3 wt% NaCl solution; scan rate, 1 mV/min.

Table 5. Kinetic parameters of the corrosion process extracted from the polarization curves.

Sample	E_{corr} (V vs. Ag/AgCl/KCl _{sat})	i_{corr} ($\mu\text{A}/\text{cm}^2$)	b_a (V/dec)	b_c (V/dec)	IE (%)
Zn	−1.00	37.10	-	0.018	-
Zn/EP	−0.97	3.84	-	0.025	89
Zn/EP-SiO ₂	−0.95	2.05	1.06	0.023	94
Zn/EP-SiO ₂ -APTES (I)	−0.93	0.95	0.56	0.043	97
Zn/EP-SiO ₂ -APTES (II)	−0.92	0.75	-	0.058	98

Moreover, there is an evident shift towards more positive potentials within the layers, resulting in enhanced performance.

4. Conclusions

The main goal of this research was to obtain epoxy-based composite coatings on zinc with enhanced anti-corrosion properties. In this regard, the effect of SiO₂ and APTES-modified SiO₂ NPs prepared using two methods on the corrosion protection performance of epoxy coatings was investigated. Based on the experimental results, several conclusions can be drawn:

- The modification of silica NPs with APTES was put in evidence by using FT-IR and TEM. FT-IR spectra confirmed that the APTES molecules attached to the terminal oxygens of SiO₂, forming terminal -NH₂ groups. The TEM images demonstrated that during the modification with APTES, the particle size decreased by approximately half.
- The composite structure was confirmed via SEM/EDS analysis, which exhibited the presence of SiO₂ and its dispersion in the EP matrix.
- The electrochemical measurements performed using the EIS and PDP methods revealed the enhanced protective effect of the composite layers against Zn corrosion and their improved stability. This can be attributed to the NPs filling the pores of the EP, thereby extending the diffusion path of the corrosive medium.
- Although all nanocomposite coatings, regardless of the filler, showed superior characteristics compared to neat EP coatings, modification of the SiO₂ NPs with APTES followed by their introduction into the epoxy resin (method I) led to weaker results than the deposits prepared through functionalization of the SiO₂ NPs in the epoxy gel before the addition of the hardener (method II).
- The composite EP-SiO₂ NP coatings are more suitable as protective layers than plain EP coatings; the first ones are more uniform, more adherent and less hydrophilic than the latter, being at the same time responsible for the better anti-corrosion properties of the coatings.

Author Contributions: Conceptualization, T.-R.O., G.S.S. and L.M.M.; methodology T.-R.O., G.S.S. and G.K.; investigation, T.-R.O. and T.T.; writing—original draft preparation, T.-R.O.; writing—review and editing, G.S.S., L.M.M. and G.K. All authors have read and agreed to the published version of the manuscript.

Funding: This research received no external funding.

Institutional Review Board Statement: Not applicable.

Informed Consent Statement: Not applicable.

Data Availability Statement: The data that support the findings of this study are available upon request from the authors.

Acknowledgments: Tamara-Rita Ovari thanks the financial support for her doctoral research provided by the Romanian Ministry of Education.

Conflicts of Interest: The authors declare no conflict of interest.

References

1. Makhlof, A.S.H. *Handbook of Smart Coatings for Materials Protection*; Elsevier: Amsterdam, The Netherlands, 2014; ISBN 9780857096807.
2. Tiwari, A.; Hihara, L.; Rawlins, J. (Eds.) *Intelligent Coatings for Corrosion Control*; Butterworth-Heinemann: Oxford, UK, 2014; pp. 59–91.
3. Muresan, L.M. Nanocomposite Coatings for Anti-Corrosion Properties of Metallic Substrates. *Materials* **2023**, *16*, 5092. [[CrossRef](#)]
4. Randis, R.; Darmadi, D.B.; Gapsari, F.; Sonief, A.A.A.; Akpan, E.D.; Ebenso, E.E. The potential of nanocomposite-based coatings for corrosion protection of metals: A Review. *J. Mol. Liq.* **2023**, *390*, 123067. [[CrossRef](#)]
5. Liu, X.; Xiong, J.; Lv, Y.; Zuo, Y. Study on corrosion electrochemical behavior of several different coating systems by EIS. *Prog. Org. Coat.* **2009**, *64*, 497–503. [[CrossRef](#)]
6. Ollik, K.; Lieder, M. Review of the Application of Graphene-Based Coatings as Anticorrosion Layers. *Coatings* **2020**, *10*, 883. [[CrossRef](#)]
7. Sari, M.G.; Shamshiri, M.; Ramezanzadeh, B. Fabricating an epoxy composite coating with enhanced corrosion resistance through impregnation of functionalized graphene oxide-co-montmorillonite Nanoplatelet. *Corros. Sci.* **2017**, *129*, 38–53. [[CrossRef](#)]
8. Hou, W.; Gao, Y.; Wang, J.; Blackwood, D.J.; Teo, S. Recent advances and future perspectives for graphene oxide reinforced epoxy resins. *Mater. Today Commun.* **2020**, *23*, 100883. [[CrossRef](#)]
9. Atta, A.M.; Ezzat, A.O.; El-Saeed, A.M.; Tawfeek, A.M.; Sabeela, N.I. Self-healing of chemically bonded hybrid silica/epoxy for steel coating. *Prog. Org. Coat.* **2020**, *141*, 105549. [[CrossRef](#)]
10. Chang, K.-C.; Lin, H.-F.; Lin, C.-Y.; Kuo, T.-H.; Huang, H.-H.; Hsu, S.-C.; Yeh, J.-M.; Yang, J.-C.; Yu, Y.-H. Effect of Amino-Modified Silica Nanoparticles on the Corrosion Protection Properties of Epoxy Resin-Silica Hybrid Materials. *J. Nanosci. Nanotechnol.* **2008**, *8*, 3040–3049. [[CrossRef](#)]
11. Conradi, M.; Kocijan, A.; Kek-Merl, D.; Zorko, M.; Verpoest, I. Mechanical and anticorrosion properties of nanosilica-filled epoxy-resin composite coatings. *Appl. Surf. Sci.* **2014**, *292*, 432–437. [[CrossRef](#)]
12. Rajabi, M.; Rashed, G.R.; Zaarei, D. Assessment of graphene oxide/epoxy nanocomposite as corrosion resistance coating on carbon steel. *Corros. Eng. Sci. Technol.* **2015**, *50*, 509–516. [[CrossRef](#)]
13. Ramezanzadeh, B.; Niroumandrad, S.; Ahmadi, A.; Mahdavian, M.; Moghadam, M.M. Enhancement of barrier and corrosion protection performance of an epoxy coating through wet transfer of amino functionalized graphene oxide. *Corros. Sci.* **2016**, *103*, 283–304. [[CrossRef](#)]
14. Parhizkar, N.; Shahrabi, T.; Ramezanzadeh, B. A new approach for enhancement of the corrosion protection properties and interfacial adhesion bonds between the epoxy coating and steel substrate through surface treatment by covalently modified amino functionalized graphene oxide film. *Corros. Sci.* **2017**, *123*, 55–75. [[CrossRef](#)]
15. Ramezanzadeh, M.; Ramezanzadeh, B.; Sari, M.G.; Saeb, M.R. Corrosion resistance of epoxy coating on mild steel through polyamidoamine dendrimer-covalently functionalized graphene oxide nanosheets. *J. Ind. Eng. Chem.* **2020**, *82*, 290–302. [[CrossRef](#)]
16. Pourhashem, S.; Rashidi, A.; Vaezi, M.R.; Bagherzadeh, M.R. Excellent corrosion protection performance of epoxy composite coatings filled with amino-silane functionalized graphene oxide. *Surf. Coat. Technol.* **2017**, *317*, 1–9. [[CrossRef](#)]
17. Keshmiri, N.; Najmi, P.; Ramezanzadeh, M.; Ramezanzadeh, B. Designing an eco-friendly lanthanide-based metal organic framework (MOF) assembled graphene-oxide with superior active anti-corrosion performance in epoxy composite. *J. Clean. Prod.* **2021**, *319*, 128732. [[CrossRef](#)]
18. Chen, L.; Chai, S.; Liu, K.; Ning, N.; Gao, J.; Liu, Q.; Chen, F.; Fu, Q. Enhanced Epoxy/Silica Composites Mechanical Properties by Introducing Graphene Oxide to the Interface. *ACS Appl. Mater. Interfaces* **2012**, *4*, 4398–4404. [[CrossRef](#)]
19. Wan, Y.-J.; Tang, L.-C.; Gong, L.-X.; Yan, D.; Li, Y.-B.; Wu, L.-B.; Jiang, J.-X.; Lai, G.-Q. Grafting of epoxy chains onto graphene oxide for epoxy composites with improved mechanical and thermal properties. *Carbon* **2014**, *69*, 467–480. [[CrossRef](#)]
20. Zou, H.; Wu, S.; Shen, J. Polymer/Silica Nanocomposites: Preparation, Characterization, Properties, and Applications. *Chem. Rev.* **2008**, *108*, 3893–3957. [[CrossRef](#)]
21. Albert, E.; Cotelan, N.; Nagy, N.; Sáfrán, G.; Szabó, G.; Muresan, L.-M.; Hórvölgyi, Z. Mesoporous silica coatings with improved corrosion protection properties. *Microporous Mesoporous Mater.* **2015**, *206*, 102–113. [[CrossRef](#)]
22. Cotelan, N.; Varvara, S.; Albert, E.; Szabó, G.; Hórvölgyi, Z.; Muresan, L.-M. Evaluation of corrosion inhibition performance of silica sol-gel layers deposited on galvanised steel. *Corros. Eng. Sci. Technol.* **2016**, *51*, 373–382. [[CrossRef](#)]
23. Szabó, G.; Albert, E.; Both, J.; Kócs, L.; Sáfrán, G.; Szöke, A.; Hórvölgyi, Z.; Muresan, L.M. Influence of embedded inhibitors on the corrosion resistance of zinc coated with mesoporous silica layers. *Surf. Interfaces* **2019**, *15*, 216–223. [[CrossRef](#)]
24. Ovari, T.-R.; Katona, G.; Coros, M.; Szabó, G.; Muresan, L.M. Corrosion behaviour of zinc coated with composite silica layers incorporating poly(amidoamine)-modified graphene oxide. *J. Solid State Electrochem.* **2023**, *27*, 1795–1811. [[CrossRef](#)]
25. Both, J.; Szabó, G.; Katona, G.; Muresan, L.M. Tannic acid reinforced sol-gel silica coatings for corrosion protection of zinc substrates. *Mater. Chem. Phys.* **2022**, *282*, 125912. [[CrossRef](#)]
26. Mehmood, S.; Ali, N.; Ali, F.; Haq, F.; Haroon, M.; Fahad, S. The Influence of Surface Modified Silica Nanoparticles: Properties of Epoxy Nanocomposites. *Z. Phys. Chem.* **2021**, *235*, 649–661. [[CrossRef](#)]

27. Kongparakul, S.; Kornprasert, S.; Suriya, P.; Le, D.; Samart, C.; Chantarasiri, N.; Prasassarakich, P.; Guan, G. Self-healing hybrid nanocomposite anticorrosive coating from epoxy/modified nanosilica/perfluorooctyl triethoxysilane. *Prog. Org. Coat.* **2017**, *104*, 173–179. [CrossRef]
28. Wang, S.; Hu, Z.; Shi, J.; Chen, G.; Zhang, Q.; Weng, Z.; Wu, K.; Lu, M. Green synthesis of graphene with the assistance of modified lignin and its application in anticorrosive waterborne epoxy coatings. *Appl. Surf. Sci.* **2019**, *484*, 759–770. [CrossRef]
29. Gao, X.; Yan, R.; Lv, Y.; Ma, H.; Ma, H. In situ pretreatment and self-healing smart anti-corrosion coating pre-prepared through eco-friendly water-base epoxy resin combined with non-toxic chelating agents decorated biomass porous carbon. *J. Clean. Prod.* **2020**, *266*, 121920. [CrossRef]
30. Irfan, M.; Iqbal, S.; Ahmad, S. Waterborne reduced graphene oxide dispersed sebacic acid modified soy epoxy nanocomposite: A green and sustainable approach for high performance mechanically robust anticorrosive coatings. *Prog. Org. Coat.* **2022**, *170*, 106984. [CrossRef]
31. Zhao, Y.; He, Y.; Yan, S.; Li, C.; Li, H.; Chen, W.; Yan, J.; Wu, G.; Yuan, X. Eco-friendly design of α -zirconium phosphate modified by phytic acid for reinforcing the corrosion resistance of waterborne epoxy coating. *Colloids Surf. A Physicochem. Eng. Asp.* **2023**, *656*, 106984. [CrossRef]
32. Measuring Adhesion by Tape Test per ASTM D3359 Issues and Challenges Behind a “Basic” Adhesion Test. Available online: [\(https://kta.com/kta-university/adhesion-astm-d3359/#:~:text=The%20scale%20ranges%20from%200,used%20\(e.g.%2C%203B\)\)](https://kta.com/kta-university/adhesion-astm-d3359/#:~:text=The%20scale%20ranges%20from%200,used%20(e.g.%2C%203B)) (accessed on 18 October 2023).
33. Karnati, S.R.; Oldham, D.; Fini, E.H.; Zhang, L. Surface functionalization of silica nanoparticles to enhance aging resistance of asphalt binder. *Constr. Build. Mater.* **2019**, *211*, 1065–1072. [CrossRef]
34. Shi, X.; Nguyen, T.A.; Suo, Z.; Liu, Y.; Avci, R. Effect of nanoparticles on the anticorrosion and mechanical properties of epoxy coating. *Surf. Coat. Technol.* **2009**, *204*, 237–245. [CrossRef]
35. Kong, X.-F.; Yang, B.; Xiong, H.; Zhou, Y.; Xue, S.-G.; Xu, B.-Q.; Wang, S.-X. Selective removal of heavy metal ions from aqueous solutions with surface functionalized silica nanoparticles by different functional groups. *J. Cent. South Univ.* **2014**, *21*, 3575–3579. [CrossRef]
36. Alipanah, N.; Yari, H.; Mahdavian, M.; Ramezanzadeh, B.; Bahlakeh, G. Fabrication of MIL-88A sandwiched in graphene oxide nanocomposites using a green approach to induce active/barrier protective functioning in epoxy coatings. *J. Clean. Prod.* **2021**, *321*, 128928. [CrossRef]
37. Scully, J.R. Electrochemical Impedance of Organic-Coated Steel: Correlation of Impedance Parameters with Long-Term Coating Deterioration. *J. Electrochem. Soc.* **1989**, *136*, 979–990. [CrossRef]
38. McIntyre, J.M.; Pham, H.Q. Electrochemical impedance spectroscopy; a tool for organic coatings optimizations. *Prog. Org. Coat.* **1996**, *27*, 201–207. [CrossRef]
39. Miszczyk, A.; Darowicki, K. Water uptake in protective organic coatings and its reflection in measured coating impedance. *Prog. Org. Coat.* **2018**, *124*, 296–302. [CrossRef]
40. Ma, I.W.; Ammar, S.; Bashir, S.; Selvaraj, M.; Assiri, M.A.; Ramesh, K.; Ramesh, S. Preparation of hybrid chi-tosan/silica composites via ionotropic gelation and its electrochemical impedance studies. *Prog. Org. Coat.* **2020**, *145*, 105679.
41. González, S.; Fox, V.; Souto, R.M. Laboratory evaluation of corrosion resistance at metallic substrates by an organic coating: Delamination effects. *J. Adhes. Sci. Technol.* **2004**, *18*, 455–464. [CrossRef]
42. Hack, H.P.; Scully, J.R. Defect Area Determination of Organic Coated Steels in Seawater Using the Breakpoint Frequency Method. *J. Electrochem. Soc.* **1991**, *138*, 33–40. [CrossRef]
43. Deflorian, F.; Fedrizzi, L.; Bonora, P. Determination of the reactive area of organic coated metals: Physical meaning and limits of the break-point method. *Electrochim. Acta* **1993**, *38*, 1609–1613. [CrossRef]
44. Ramezanzadeh, B.; Haeri, Z.; Ramezanzadeh, M. A facile route of making silica nanoparticles-covered graphene oxide nanohybrids (SiO₂-GO); fabrication of SiO₂-GO/epoxy composite coating with superior barrier and corrosion protection performance. *Chem. Eng. J.* **2016**, *303*, 511–528. [CrossRef]
45. Razin, A.A.; Ramezanzadeh, B.; Yari, H. Detecting and estimating the extent of automotive coating delamination and damage indexes after stone chipping using electrochemical impedance spectroscopy. *Prog. Org. Coat.* **2016**, *92*, 95–109. [CrossRef]

Disclaimer/Publisher’s Note: The statements, opinions and data contained in all publications are solely those of the individual author(s) and contributor(s) and not of MDPI and/or the editor(s). MDPI and/or the editor(s) disclaim responsibility for any injury to people or property resulting from any ideas, methods, instructions or products referred to in the content.